

SASIA3D: A 3-D CRUST AND UPPER-MANTLE VELOCITY MODEL OF SOUTH ASIA DERIVED FROM JOINT INVERSION OF P-WAVE TRAVEL TIMES AND SURFACE-WAVE DISPERSION DATA

William L. Rodi¹ and Delaine T. Reiter²

Massachusetts Institute of Technology, Earth Resources Laboratory¹ and Weston Geophysical Corp.²

Sponsored by Air Force Research Laboratory

Contract No. FA8718-04-C-0027

ABSTRACT

Accurate travel-time predictions for regional seismic phases are essential for locating small seismic events with the accuracy needed for nuclear monitoring decisions. Travel times calculated through a three-dimensional (3-D) Earth model have the best chance of achieving acceptable prediction errors, if the model is constrained by sufficient data. With this motivation, we have developed a self-consistent 3-D P and S velocity model of the crust and upper mantle in a large region of southern and central Asia to a depth of approximately 400 km. The new model, which we are calling *SAsia3D*, is the result of a nonlinear, joint body-wave/surface-wave inversion method applied to Pn travel times collected from the Engdahl, van der Hilst and Buland (EHB) bulletin and group-velocity measurements provided by groups at the University of Colorado and Lawrence Livermore National Laboratory. Consistency between the P and S velocities is achieved by imposing bounds on Poisson's ratio and by invoking a regularization constraint that correlates variations in P and S velocity from an initial model. We have begun validating *SAsia3D* through relocation of ground-truth events in the study area using regional phase arrivals. The location validation exercises indicate that in many cases our 3-D model achieves excellent epicentral accuracy. Most notably, *SAsia3D* performs well when both regional P and S phase arrivals are included in the location. The regional P/S locations obtained with *SAsia3D* are frequently superior to the locations obtained with a large set of teleseismic and regional P arrivals and the AK135 reference model.

OBJECTIVES

The development and validation of accurate 3-D velocity models of the crust and upper mantle for regions of nuclear monitoring interest remain important goals for nuclear monitoring organizations. Systematic biases caused by inadequately modeled Earth structures cause errors in the estimation of geophysical parameters such as the travel times and amplitudes of regional seismic phases. More accurate and reliable estimates of these quantities (especially in aseismic regions) will improve nuclear monitoring efforts to detect, locate and discriminate regional events. Therefore, we have developed a joint 3-D inversion technique that incorporates both compressional-wave travel times and Rayleigh-wave group velocity measurements to determine the full P and S velocity structure of the crust and upper mantle.

In this paper we report on the development of a new model, *SAsia3D*, derived from data observed in the broad region shown in Figure 1. This region, extending from 10°–50° N and 40°–110° E, covers some of the most tectonically complex areas on Earth.

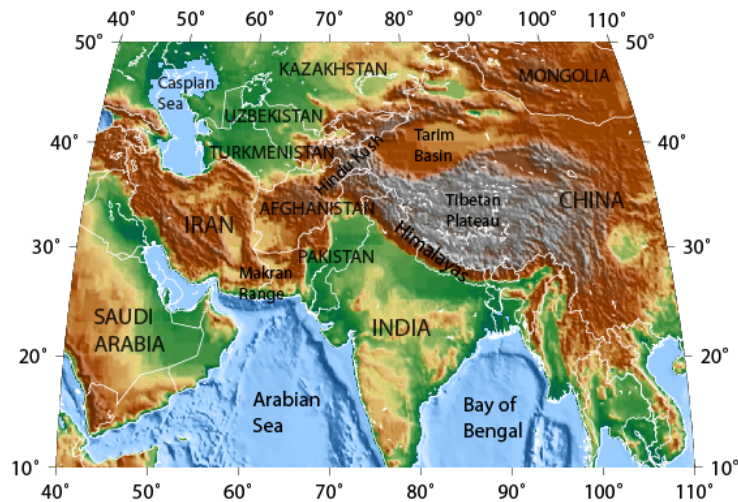


Figure 1. Topographic map of study region, which encompasses most of central and southern Asia, as well as portions of the Middle East.

RESEARCH ACCOMPLISHED

Body-wave (Travel-Time) and Surface-Wave (Rayleigh Dispersion) Data Sets

Compressional-wave travel-time database

The travel times we use in the P -wave tomography are taken from the EHB bulletin (Engdahl et al., 1998). We extracted arrivals from 1988–2004 having event and station locations within 0°–60°N, 30°–120°E and event depths between 0 and 200 km, including only first-arriving phases denoted P_g , P_b or P_n and which were defining phases for the EHB locations. To ensure small epicentral mislocations in the events, we required the secondary azimuth gap for a given event to be less than or equal to 130° (Bondár et al., 2004) and the number of teleseismic arrivals to be at least 15. The data set satisfying these criteria comprised 124,080 arrivals from 6,079 events and 735 stations.

We compressed this data set by forming summary events on a regular grid having 0.5° spacing in latitude and longitude and containing 13 nodes in depth between 0 and 200 km, with the depth spacing per node increasing from 5 to 20 km. For each summary-event node and each station/phase type, a summary travel-time residual (relative to the AK135 Earth model) was formed by averaging the individual residuals for the events near that node. Following this compression, stations containing fewer than 25 arrivals were dropped from the data set. The use of summary events acknowledges the redundant sensitivity of individual data to the Earth model (which is on 1° grid) and, combined with the station-dropping rule, reduces the ray-tracing requirements for the inversion substantially.

The final database used in the body-wave tomography contained 76,355 arrivals for 2,998 summary events and 438 stations. The data spanned epicentral distances to 18.7 degrees, and the travel-time residuals (relative to AK135) ranged from -8.0 to 8.8 s with a root-mean-square (RMS) residual error of 2.5 s. The path coverage for the travel-time database is shown on the left in Figure 2; it demonstrates that we have excellent coverage for nearly our entire study region, with the exception of the eastern tip of Saudi Arabia, where there is low seismicity and a lack of station coverage.

Surface-wave dispersion database

The surface-wave dispersion database was collected from several sources, but primarily consists of measurements made by the University of Colorado at Boulder (CUB) group (Ritzwoller and Levshin, 1998) and the Lawrence Livermore National Laboratory (Pasyanos, personal communication). Some measurements in the region were also made by the Weston Geophysical internal group. To eliminate potential outliers in the data set, we performed a period-by-period grooming of the data, in which we retained a group velocity measurement if it was within two standard deviations of the mean group velocity for that period. This exercise resulted in a database of 97,548 fundamental-mode Rayleigh group velocity picks from 3,847 events, 170 stations and 23 periods: $T = 10\text{--}16, 18, 20, 25, 30, 35, 40, 50, 60, 70, 80, 90, 100, 120, 125, \text{ and } 150$ s. A depiction of the great-circle path coverage over our study region is shown on the right in Figure 2.

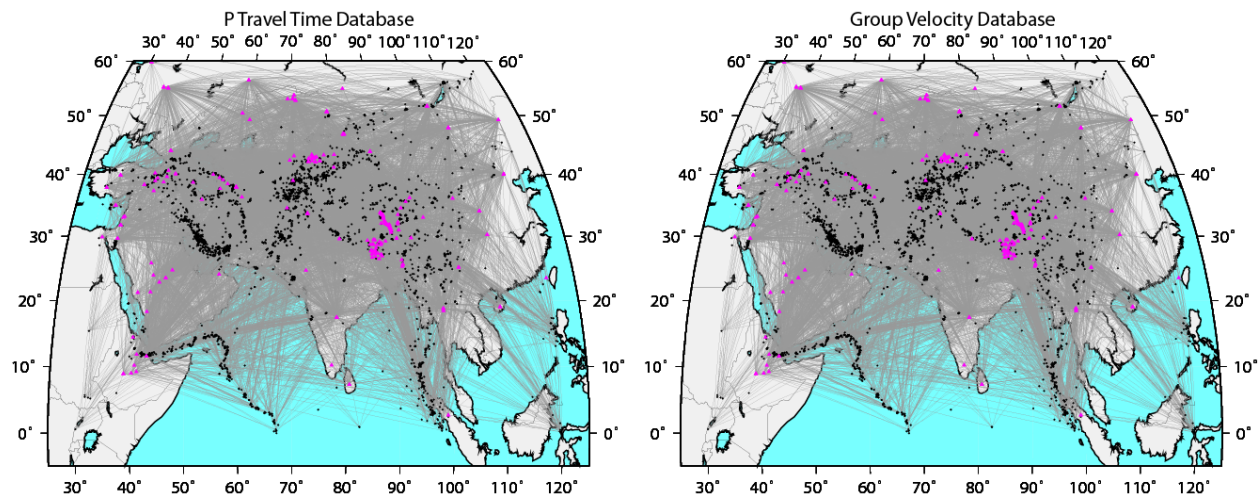


Figure 2. Path coverage for the summary-event *P*-wave travel-time (left) and surface-wave dispersion (right) data sets, displayed with great-circle rays between event and station locations. Purple triangles represent stations, and black dots are the summary-event (travel times) or event (group velocity) locations.

Model Parameterization and Initial Model

We parameterize a 3-D Earth model as a geographic grid of independent 1-D models, each comprising a *P* and *S* velocity (and density, for purposes of dispersion modeling) function versus depth. A 1-D model is specified by the velocities and depths of a fixed number of vertical nodes. Linear interpolation of velocities between nodes vertically, and of velocities and depths laterally, defines a complete spatial 3-D model.

The vertical nodes of the model are segregated into distinct “units” separated by velocity discontinuities. We selected these units based on the CRUST2.0 (Bassin et al., 2000) and AK135 (Kennett et al., 1995) models. The crust thus has seven units with each taken as a vertically homogeneous layer (sometimes of zero thickness): ice, water, soft sediment and hard sediment overlying three deeper crustal layers (nominally granitic, intermediate, and basaltic). The mantle has a single upper mantle unit between the Moho and 410 kilometers, underlain by a transition zone unit (410–660 km) and a single lower mantle unit (660–2891.5 km).

The free parameters in our joint inversion are the *P* and *S* velocities of the main crustal units (granitic through

basaltic) and of the mantle to a depth of 410 km. The mantle velocities are sampled at nine vertical nodes. An additional free parameter of the model is the Moho depth, which we adjust in the surface-wave inversion part of our inversion procedure. Moho adjustments are accommodated by proportionate thickening or thinning of the main crustal units.

The initial model for our joint inversion is a composite 3-D model consisting of the CRUST2.0 model for the crust and the 1-D AK1355 reference model for the mantle. The CRUST2.0 Pn velocities were ignored in favor of the AK135 velocities ($V_P = 8.04$ km/s, $V_S = 4.48$ km/s at the top of the mantle). However, the CRUST2.0 variable Moho depth was retained and accommodated by vertical compression or extension of the AK135 mantle thickness to a depth of 210 km.

Inversion Method

We have developed an algorithm that performs a joint, nonlinear inversion of body-wave travel times and surface-wave group delays to obtain fully 3-D regional models of the crust and upper mantle. Problem nonlinearity is handled by iterating over linearized inversion steps, with the aid of finite-difference ray tracing techniques to perform the necessary forward modeling in the updated Earth model at each iteration step.

At each step of the iteration, we perform linearized body-wave and surface-wave inversion as separate procedures. The body-wave data, comprising only first-arrival P -wave times, are used to update the P velocity model (V_P). The surface-wave dispersion data are used to update the S -wave model (V_S) in a two-step procedure, ignoring the small dependence of Rayleigh wave dispersion on P velocity. This sequential approach allows us to avoid some of the pitfalls associated with large simultaneous inverse problems. However, the separate inversions are coupled through the prior information applied to their respective velocity models.

The prior information used in each linearized inversion is of two types. First, we apply constraints on the size and spatial smoothness of velocity perturbations using a Tikhonov regularization approach (Tikhonov and Arsenin, 1977). The Tikhonov stabilizing functional in our case is based on a geostatistical formulation, whereby a prior variance and horizontal and vertical correlation distances are used in lieu of a simple regularization parameter (see Rodi et al., 2005). The second form of prior information consists of upper and lower bounds on the P and S velocities, which are allowed to vary with depth and tectonic regime. The velocity bounds are determined in part from bounds on Poisson's ratio. We describe some key aspects of the body-wave and surface-wave linearized inversion algorithms in the paragraphs below and refer the reader to Reiter and Rodi (2006) for additional details.

Body-Wave Inversion: At each step of the nonlinear iteration, the linearized travel-time tomography problem is solved using travel-time sensitivities calculated from the P velocity model of the previous step (beginning with the initial model). An updated 3-D P velocity model is fit to the current travel-time residuals, in a least-squares sense, subject to velocity bounds and geostatistical constraints. The velocity bounds combine a priori bounds on P velocity and on Poisson's ratio. The latter are used to map the current S velocity model, point by point, to an acceptable range of P velocities.

The P velocity update minimizes an objective function that sums data misfit and stabilizing functions, the latter embodying the geostatistical constraints. Velocity bounds are implemented with the use of a parameter mapping technique that solves directly for an unconstrained variable that is mapped onto a finite range of velocity values. This mapping technique changes the damped least-squares problem from a linear to a nonlinear one, even though the forward problem is linearized. We use a nonlinear conjugate gradients technique to obtain the solution.

The body-wave tomography results shown in this paper were obtained with the following choices of geostatistical parameters. The prior standard deviation of V_P , at each point in the model, was set to 1% of the initial model velocity at that point. The correlation distances for the mantle velocity were 300 km and 60 km in the horizontal and vertical directions, respectively. In the crust, the horizontal correlation distance was also 300 km, but the vertical correlation distance was set to half the crustal thickness. Velocities in the crust and upper mantle were de-correlated, i.e., no smoothing was applied across the Moho discontinuity.

Surface-wave inversion

We solve the linearized surface-wave inversion problem using a two-part solution. The first part entails fitting group velocity maps, one for each period, to the observed group delays over source-receiver paths. This tomography problem uses sensitivities obtained by applying 2-D finite-difference ray tracing to the *phase* velocity maps predicted by the V_P/V_S model of the previous iteration step. To produce an updated set of group velocity maps we employ the same tomography technique that is used to invert the body-wave travel times. The data are now the observed group delays and the 3-D model parameter is now group velocity as a function of latitude, longitude and period. The depth coordinate used in the body-wave tomography is replaced with logarithmic period, with an appropriate correlation “distance” assigned to accomplish some degree of smoothing over period (10% of the period in the results presented here). With regard to the other geostatistical parameters, the results presented here used a horizontal correlation distance of 300 km, as in the body-wave tomography, while the prior standard deviation of group velocity was set to 2% of the initial model values. A departure from the body-wave tomography technique is that group-velocity bounds were set very wide so as to have minimal effect on the solution; we did not derive the bounds that are implied by the shear-velocity bounds for the Earth.

Following the tomographic inversion of the group delays to retrieve a set of group-velocity maps at the set of twenty-three observation periods, we can extract an individual dispersion curve as a function of period from the maps, appropriate for any latitude/longitude point in our model grid. Applying a 1-D inversion method to the dispersion curve yields a V_S profile as a function of depth for the geographic point, and repeating this process for the whole model grid results in a 3-D S -wave velocity model. We solve the 1-D inversion problem by minimizing an objective function similar to that used in the P -wave travel-time tomography. The stabilizing function term imposes geostatistical smoothing, and minimization is subject to upper and lower S velocity bounds, including bounds inferred from Poisson’s ratio bounds and the current V_P model. We also restrict the model to allow changes only in certain “depth zones,” depending on the confidence we have in the resolving power of the dispersion data. As with the travel-time tomography, we employ the previously described parameter mapping technique to enforce the velocity bounds, but this time we use Gauss-Newton iteration to deal with the ensuing nonlinearity.

The shear-wave inversion results shown here were obtained with the following choices for smoothing parameters. The prior standard deviation of V_S was set to 3% of the average reference model velocity in the crustal layers and 2% in the mantle layers. As in the P -wave tomography, the vertical correlation distance was one-half of the crustal thickness and 60 km in the upper mantle. No smoothing was applied across the Moho discontinuity.

The biggest departure of our S -wave inversion technique from our P -wave tomography technique is that Moho depth is a free parameter in the former, acknowledging the sensitivity of group velocities at the observed periods to this parameter. The inversion for Moho depth is accomplished via grid search, with the S -wave inversion performed for each trial depth and the value achieving the smallest objective function taken as the solution. The Moho-depth grid spanned crustal thickness changes of -10% to $+15\%$ in steps of 5%.

In the next sections we present some results of performing four iterations of the joint inversion technique.

Joint Inversion Results

V_p and V_s models

In Figure 3 we show horizontal slices in the upper mantle through the *SAsia3D* model as a percent deviation from the AK135 model velocity at depths of 120, 210, 260, and 310 km. There is spatial correlation between the V_P and V_S models, but not as much in the upper mantle as in the crust (not shown). The primary observation to note in Figure 3 is the progressive slowing of the model as the depth increases, in both V_P and V_S . This suggests that the positive velocity gradient in the AK135 upper mantle is not consistent with our travel-time or dispersion data sets.

Figure 4 shows two vertical slices through the *SAsia3D* model along great-circle paths. The results are again shown as percent deviation from the initial model (i.e., CRUST2.0 over the AK135 mantle). We note that the percent deviation of the crust from its 3-D initial model is calculated with respect to an average 1-D model at a particular latitude-longitude point. On the left is a slice across the Saudi Arabian Peninsula to the northeast across southeastern Iran and into eastern Kazakhstan. The slice on the right has endpoints at 30° N latitude, stretching from western Iran

into central China. The predominant feature in the slices are the high velocity (with respect to the background model) areas beneath known areas of orogeny, such as the Makran in southern Iran and the Hindu Kush/Pamir in northern Afghanistan and western China. The V_P model shows these subsurface features most clearly, while the V_S model only hints at their outlines. There is also an interesting low velocity feature in both the V_P and V_S models beneath central Iran, which may have interesting implications for the active subduction processes occurring beneath the Eurasian continental collision zone.

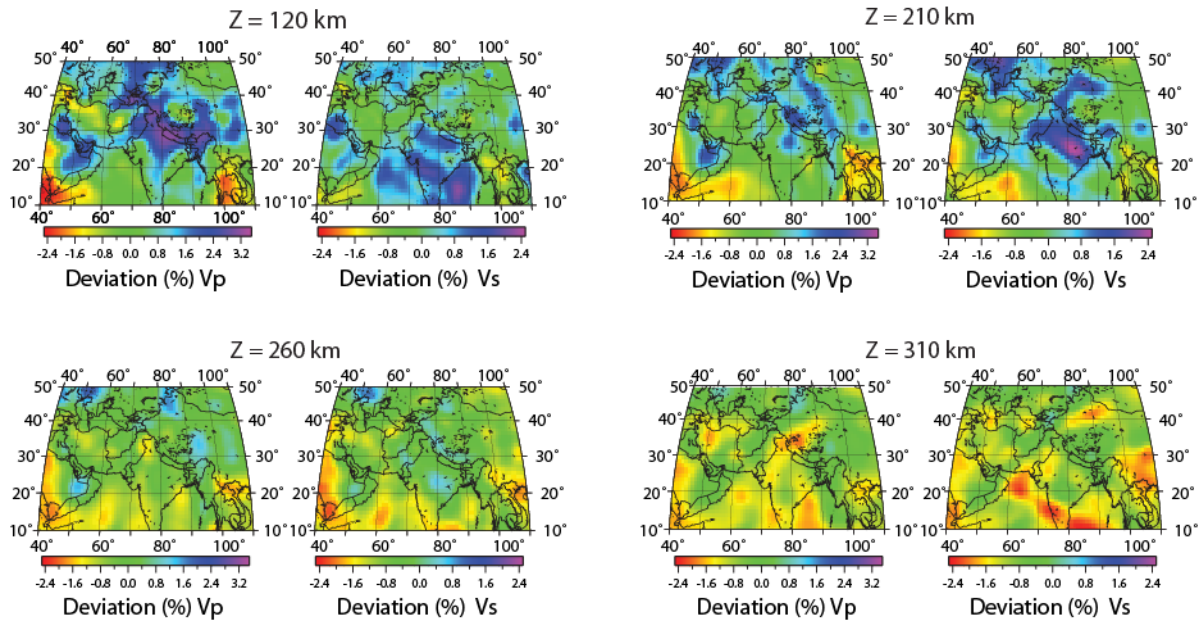


Figure 3. Results from the *SAsia3D* joint inversion model. Each subplot shows a slice at a given upper-mantle depth of V_P and V_S . The results are given as percent deviation from the AK135 velocity model at the slice's depth. The *SAsia3D* model tends toward lower velocities as the depth increases (e.g., 260- and 310-km depth slices).

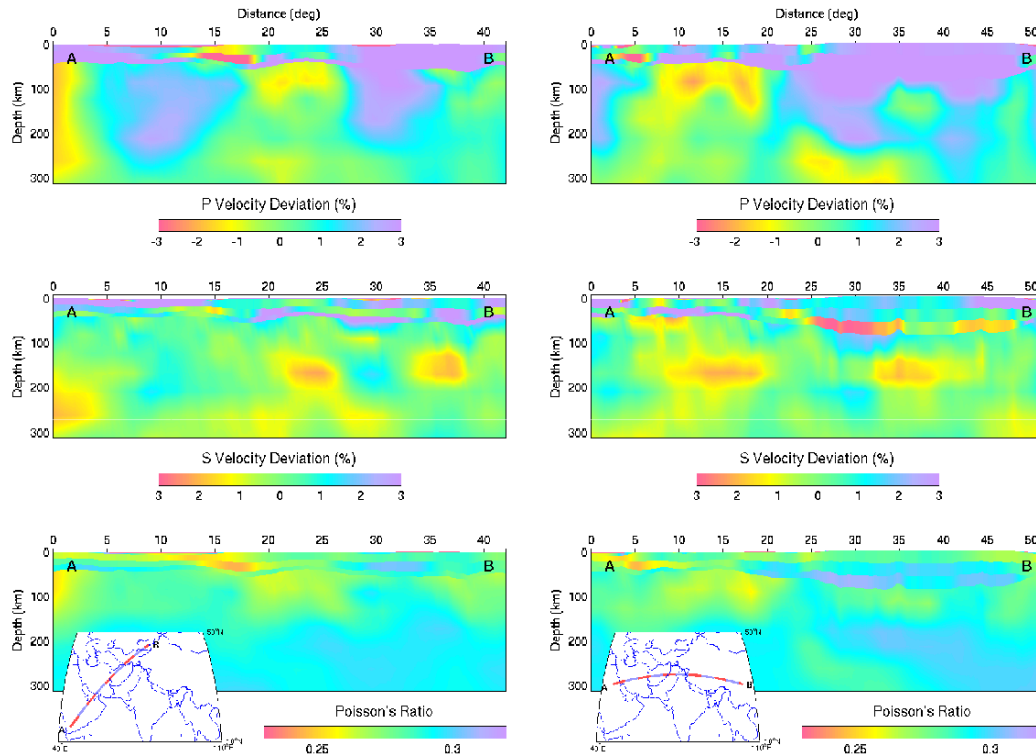


Figure 4. Two vertical slices for V_P (top), V_S (middle) and Poisson's ratio (bottom) through the *SAsia3D* joint model along great-circle paths. The results are shown as a percent deviation from the initial model (i.e., CRUST2.0 over an AK135 mantle).

Group velocity maps

One of the important corollary products of the inversion is a predicted set of group-velocity maps. Group velocities can be used to construct phase-matched filters in combination with regional surface-wave magnitude formulas to improve the m_b : M_s discriminant and extend it to smaller magnitudes (Pasyanos et al., 2004). We show the group velocity results at a period of 30 s predicted through the *SAsia3D* model in Figure 5 for the inversion region of 10° – 50° N and 40° – 110° E. We also show two zoomed views comparing *SAsia3D* with other recently published group-velocity maps. The two models for which we have results include those published by Pasyanos and Walter, 2002, and Mitra et al., 2005.

In general, comparison of our group velocity maps with those of the other authors indicates good agreement on most long-wavelength features, with differences restricted to smaller-scale features and specific velocity variations. We do note that at higher periods (not shown) the *SAsia3D* group velocities tend to be lower than those in the other models. It is not clear yet what is causing this phenomenon.

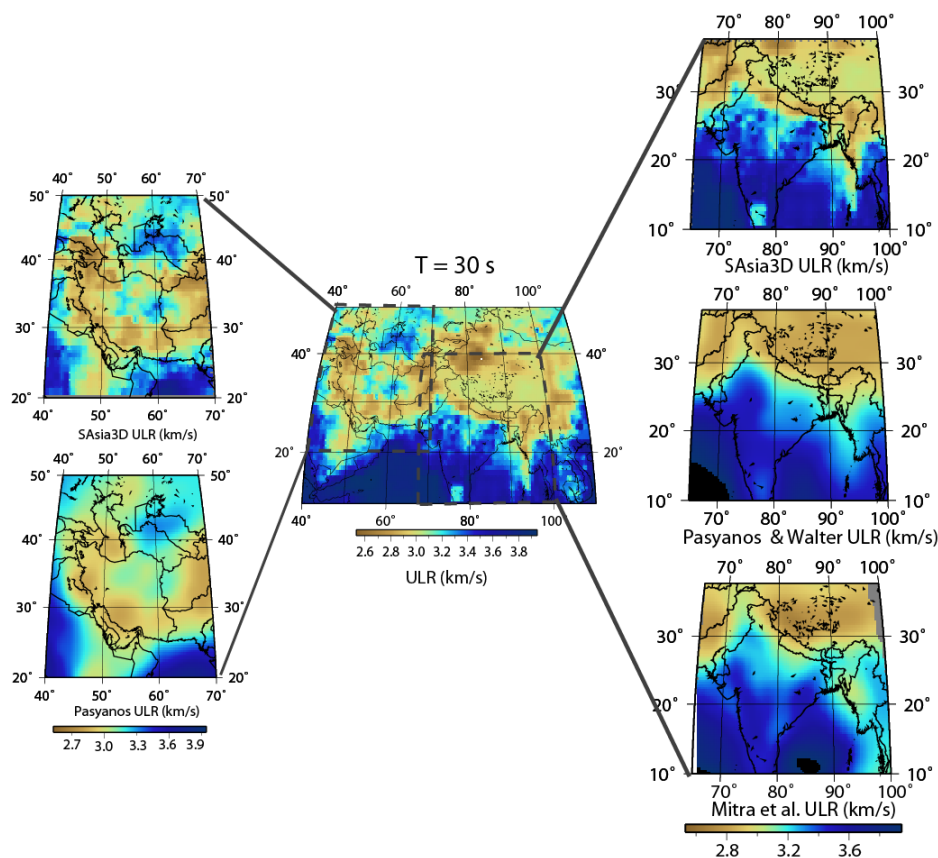


Figure 5. Predicted group velocities from SAsia3D at a period of 30 s. The middle plot shows the group-velocity map across our entire study region. The zoomed views on the left and right compare SAsia3D to models from Pasyanos and Walter (2002) and Mitra (2005). SAsia3D exhibits a slight shift to lower velocities, but overall the spatial patterns across the models are similar.

Validation Exercises

We have begun to validate the new *SAsia3D* model by relocating a ground-truth (GT) database of explosions and shallow earthquakes in the region (Bondár et al., 2004), and by comparing the travel-time predictions for the arrivals in the database within the boundaries of our region. Our initial location validation has been done using the event list published by Engdahl (2006) for the ISC Location Workshop held at the International Association of Seismology and Physics of the Earth's Interior (IASPEI) General Assembly in Santiago, Chile, in 2005. A filtering of that event database results in 10 explosions and 13 earthquakes within our region, with 833 *Pn* or *P* arrivals and 145 *Sn* or *S* arrivals. Figure 6 shows the locations of our initial validation events, color-coded according to the secondary azimuth gap of the regional arrivals.

We use the Grid-search Multiple-Event Location (GMEL) algorithm (Rodi, 2006) to perform our validation experiments. The goal of these experiments is to compare epicentral mislocations and travel-time residuals achieved with the new 3-D velocity model to the mislocations and residuals achieved with either our initial 3-D model or a standard 1-D reference model (in this case, AK135). The results are compiled in Figure 7, which is divided into mislocation comparisons in Figure 7a and the travel-time prediction results in Figure 7b. The event relocation experiments were run with event depths fixed to their reported values.

Each plot in Figure 7a tells a specific story about the ability of the *SAsia3D* model to improve the locations of the ground-truth (GT) events over the AK135 reference model and our starting model. The top left plot in Figure 7a shows that, in comparison to AK135, *SAsia3D* does a significantly better job of locating the GT events. There are more events on the “3-D Wins” side of the plot because the 3-D mislocations are closer to the zero axis. In contrast,

the top right subplot illustrates that the starting model (CRUST2.0 over AK135 mantle) does not decrease the GT mislocations over AK135 in any significant way.

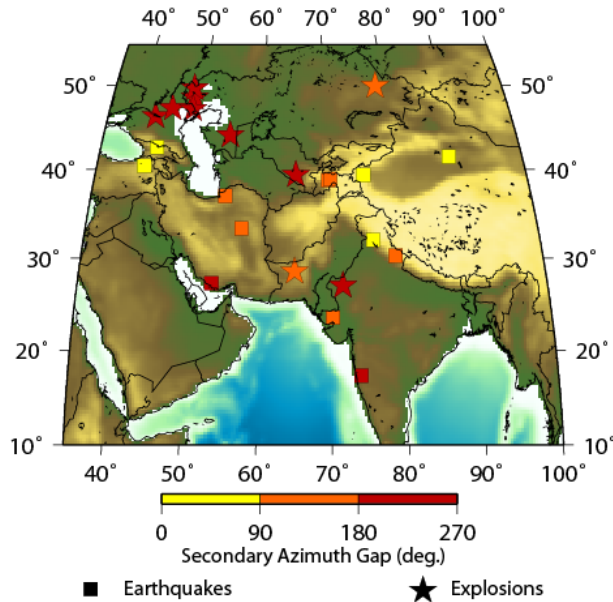


Figure 6. Reference-event (GT0–GT5) database from Engdahl (2006) within the confines of our study region. The events are color-coded by their secondary azimuth gap for the regional phases we used for relocation, which provides a measure of the network coverage bias.

The bottom two plots in Figure 7a should also be compared to the top left subplot. In the bottom left plot, we show the effect of changing from an L2 norm to an L1 norm in the location misfit criterion. We included this plot to illustrate that switching the norms from L2 to L1 (which should help to decrease the effect of a bad model in a location) does not compensate for the use of AK135 in the relocations. In other words, *SAsia3D* still produces lower mislocations than the 1-D model, even when the L1 norm is used. Lastly, the bottom right plot in Figure 7a shows the results of including the additional 145 *Sn* and *S* arrivals in the GT database, compared to the results from the 1-D model with all arrivals. In this case the results indicate that the addition of *S* arrivals helps AK135 more than *SAsia3D*, particularly for two poorly located earthquakes, but *SAsia3D* overall has systematically smaller mislocations than AK135, as when only *P* arrivals were used.

Figure 7b shows the travel-time residuals for the 833 *Pn* or *P* residuals (top) and the 145 *Sn* or *S* residuals (bottom) in our GT bulletin with respect to the AK135 (purple) and *SAsia3D* (green) models. The results show that *SAsia3D* produces a better fit for the *P*-wave residuals, shifting the mean closer to zero and decreasing the spread of residuals at most distances (there is still a slight negative bias at approximately 13°–15°). The *S*-wave residuals also exhibit a reduced bias, but only out to ~6°, past which there is a strong negative shift from the AK135 residuals. We are investigating the cause of this behavior, which may have a number of explanations.

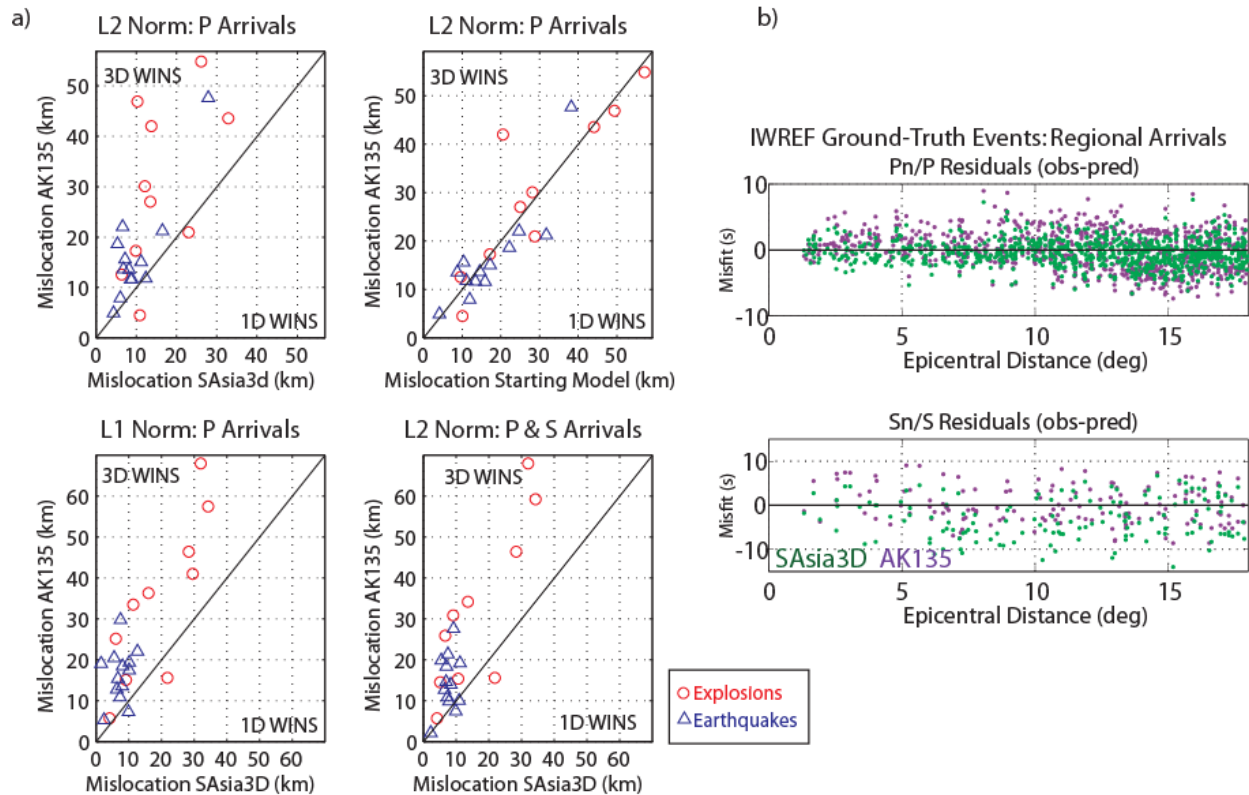


Figure 7. (a) Location validation results, shown as explosion (red triangles) or earthquake (blue circles) epicentral mislocation for the 1-D AK135 reference model versus the starting inversion model or *SAsia3D*. The details about the four subpanels are in the text. (b) The *P* and *S* regional travel-time residuals from the GT data set for the AK135 model (purple dots) and the *SAsia3D* model (green dots).

CONCLUSIONS AND RECOMMENDATIONS

We have completed the development of a new V_P and V_S model for central and southern Asia called *SAsia3D* using a new joint inversion technique that incorporates *P*-wave travel times and Rayleigh-wave group velocity data. The model has, in initial location validation exercises, proved to be very successful at locating ground-truth events with regional observations compared to both the AK135 reference model and the starting 3-D model.

The remaining tasks in this effort will include further location validation exercises using a larger set of ground-truth events. We will also test the accuracy of the group-velocity maps for predicting the observations used in m_b :*M*_s calculations, and perform a limited amount of full-waveform modeling to check the ability of *SAsia3D* to predict the kinetic behavior of both body waves and surface waves.

REFERENCES

- Bassin, C., G. Laske and G. Masters (2000). The current limits of resolution for surface wave tomography in North America, *EOS Trans AGU* 81: F897.
- Bondár, I., E. R. Engdahl, X. Yang, H. A. A. Ghalib, A. Hofstetter, V. Kirichenko, R. Wagner, I. Gupta, G. Ekström, E. Bergman, H. Israelsson, and K. McLaughlin (2004). Collection of a reference event set for regional and teleseismic location calibration, *Bull. Seis. Soc. Am.* 94: 1528–1545.
- Bondár, I., S. C. Myers, E. R. Engdahl, and E. A. Bergman (2004). Epicentre accuracy based on seismic network criteria, *Geophys. J. Int.* 156: 483–496.

29th Monitoring Research Review: Ground-Based Nuclear Explosion Monitoring Technologies

- Engdahl, E. R. (2006). Application of an improved algorithm to high precision relocation of ISC test events, *Phys. Earth Planet. Interiors* 158: 14–18.
- Engdahl E. R., R. van der Hilst, and R. Buland (1998). Global teleseismic earthquake relocation with improved travel times and procedures for depth determination, *Bull. Seis. Soc. Am.* 88: 722–743.
- Kennett, B. L. N., E. R. Engdahl, and R. Buland (1995). Constraints on seismic velocities in the Earth from travel times, *Geophys. J. Int.* 122: 108–124.
- Mitra, S., K Priestley, A. J. K. Bhattacharyya, and V. K. Gaur (2005). Crustal structure and earthquake focal depths beneath northeastern India and southern Tibet, *Geophys. J. Int.* 160: 227–248.
- Pasyanos, M. E. and W. R. Walter (2002). Crust and upper-mantle structure of North Africa, Europe and the Middle East from inversion of surface waves, *Geophys. J. Int.* 149: 463–481.
- Pasyanos, M. E., W. R. Walter, and S. E. Hazler (2004). A surface wave dispersion study of the Middle East and North Africa for monitoring the Comprehensive Nuclear-Test-Ban Treaty, *Pure Appl. Geophys.* 158: 1445–1474.
- Ritzwoller, M. H. and A. L. Levshin (1998). Eurasian surface wave tomography: Group velocities, *J. Geophys. Res.*, 103: 4839–4878.
- Reiter, D. and W. Rodi (2006). Crustal and upper-mantle P- and S-velocity structure in central and southern Asia from joint body-and surface-wave inversion, in Proceedings of the 28th Seismic Research Review: Ground-Based Nuclear Explosion Monitoring Technologies, LA-UR-06-5471, Vol. 1, pp. 209–218.
- Rodi, W. (2006). Grid-search event location with non-Gaussian error models, *Phys. Earth. Planet. Int.* 158: 55–66.
- Rodi, W., C. A. Schultz, G. Johannessen, and S. C. Myers (2005). Grid-search location methods for ground-truth collection from local and regional seismic networks, *Final Technical Report to National Nuclear Security Administration, Dept. of Energy, Contract Nos. DE-FC03-01SF22397 and W-7405-ENG-48.*
- Tikhonov, A. N. and V. Y. Arsenin (1977). *Solutions of Ill-Posed Problems*. Washington, D.C.: V. H. Winston and Sons.